

Efficient Large-Scale, Targeted Gravitational-Wave Probes of Supermassive Black-Hole Binaries

Maria Charisi^{1,*}, Stephen R. Taylor¹, Caitlin A. Witt^{2,3}, and Jessie Runnoe¹

¹*Department of Physics and Astronomy, Vanderbilt University, 2301 Vanderbilt Place, Nashville, Tennessee 37235, USA*

²*Center for Interdisciplinary Exploration and Research in Astrophysics (CIERA), Northwestern University, Evanston, Illinois 60208, USA*

³*Adler Planetarium, 1300 S. DuSable Lake Shore Drive, Chicago, Illinois 60605, USA*



(Received 5 April 2023; revised 27 October 2023; accepted 21 November 2023; published 5 February 2024)

Binary systems of supermassive black holes are promising sources of low-frequency gravitational waves (GWs) and bright electromagnetic emission. Pulsar timing array GW searches for individual binaries have been limited to only a few candidate systems due to computational demands, which get worse as more pulsars are added. By modeling the GW signal using only components from when the GW passes Earth (rather than also each pulsar), we find constraints on the binary's total mass and GW frequency that are similar to a full signal analysis, yet ~ 70 times more efficient.

DOI: 10.1103/PhysRevLett.132.061401

Introduction.—All major pulsar timing array (PTA) collaborations [1–6] have now reported evidence for a stochastic background of gravitational waves [7–10]. This was achieved by measuring coherent deviation in the arrival time of pulsar signals that are correlated among all pulsars with a quasisquadrupolar pattern (i.e., the Hellings and Downs curve [11]). The most likely origin of this background is a population of supermassive black-hole binaries (SMBHBs) [12,13]. These systems naturally form in galaxy mergers [14] and at the final stages of their evolution become promising PTA sources [15,16].

Strong gravitational-wave (GW) signals from massive and relatively nearby SMBHBs can be resolved on top of the GW background. This may occur as early as the next few years [17–21]. PTAs will detect SMBHBs thousands of years before coalescence ($\sim 10^4$ years for an equal-mass binary with $10^9 M_\odot$ and period of a few years), which likely show no evolution over the baseline of timing observations (\sim decades). Recent PTA datasets have provided upper limits on the GW strain from individual SMBHBs [22–29], including stringent mass-ratio limits on tentative SMBHBs in nearby galaxies [30,31]. Furthermore, SMBHBs may reach the GW regime embedded in gas-rich environments [32]. Therefore, in addition to GWs, they likely produce bright electromagnetic (EM) emission [33,34], making them excellent targets for multimessenger observations [35,36]. Combined EM + GW searches are very advantageous as they improve the GW upper limits [37,38], boost the GW detection probability [39], and can significantly improve parameter estimation [40,41]. Since EM observations provide very precise locations and redshifts, multimessenger searches are by default targeted toward specific galaxies of interest. This has important implications on the PTA GW data analysis, since the sky location and

luminosity distance can be fixed, unlike the typical PTA searches, which are all sky and use a broad, weakly informative prior for the distance.

In this Letter, we address a major limitation of current approaches to targeted PTA GW searches, namely, the scaling of the parameter space with the pulsar array size and the associated computational complexity. Timing deviations induced by GWs from a SMBHB include two components: (1) the Earth term, which is common in all pulsars (up to directional sensitivity factors) (e.g., [42]), and (2) the pulsar terms, which are different in each pulsar, reflecting the GW phase upon passing each one. Modeling the pulsar term is crucial for localizing the source [42,43], but makes these searches complicated and computationally expensive, because, in addition to the standard binary parameters, they also search over multiple parameters for each pulsar (pulsar distance and pulsar-term GW phase) [44]. Hence, the number of parameters needed to fully model a single SMBHB signal scales linearly with the number of pulsars in the array. Given that (i) current searches of this variety can take approximately weeks on modern CPU architectures (although efforts are being made to speed this up [45]), (ii) pulsars are being added every year to datasets, and (iii) in the future we may want to target multiple candidates simultaneously, strategies are needed to bypass current limitations and, at minimum, provide a rapid first assessment of GW candidate viability.

Indeed, for *targeted* searches, in which the candidate source location is determined by EM data, we find that modeling only the Earth term offers a significantly simpler and more computationally efficient alternative while retaining the most valuable information for multimessenger assessment. This will be extremely crucial both for GW follow-ups targeting the flood of EM candidates in the era

of the Legacy Survey of Space and Time (LSST) of the Vera Rubin Observatory [34,46–48] and for following up the hundreds or thousands of potential host galaxies within the large localization volume of a GW-triggered detection [49]. Here, we use realistic binary simulations and compare the parameter estimation and computational efficiency of Bayesian analyses that model the full signal likelihood versus ones that neglect the pulsar terms.

GW signals and simulations.—The timing deviations s induced by a binary can be written as $s(t, \hat{\Omega}) = F^+(\hat{\Omega})\Delta s_+(t) + F^\times(\hat{\Omega})\Delta s_\times(t)$, where $\hat{\Omega}$ is the GW unit position vector, $+$, \times refer to the GW polarization, $F^{+\times}$ are the antenna pattern functions that describe the response of an Earth-pulsar system to the GW signal, and

$$\Delta s_{+, \times}(t) = s_{+, \times}(t) - s_{+, \times}(t_p) \quad (1)$$

is the difference between the Earth and the pulsar term, which depends on the binary parameters, pulsar distance L , pulsar-term GW phase, and $t_p = t - L(1 - \hat{\Omega} \cdot \hat{p})$, with \hat{p} as the unit position vector of the pulsar. For a derivation of the full signal and PTA likelihood, see Refs. [25,28].

Following the framework developed in Pol *et al.* [50], we simulate timing data for a PTA with near-future sensitivity. The simulated data have a baseline of 20 years, (roughly the expected timeline for detection of GWs from individually resolved binaries [17–21]), but otherwise resemble the NANOGrav’s 12.5-yr dataset [51] in terms of number of pulsars, observational sampling, time of arrival (TOA) uncertainties etc. We also simulate intrinsic red noise for each pulsar according to its measured characteristics in the NANOGrav 12.5-yr dataset. For the extrapolated data, we keep the observational properties similar to the 12.5-yr dataset (see Ref. [50] for details). This represents a conservative choice for the future PTA sensitivity, since the number of pulsars will certainly increase. We inject one circular SMBHB signal into each of these simulated PTA datasets, randomly drawing the binary parameters from uniform distributions in the following ranges: sky location, $\theta: [0, \pi]$ and $\phi: [0, 2\pi]$; distance, $\log_{10}(D/\text{Mpc}): [1, 3]$; total binary mass, $\log_{10}(M_{\text{tot}}/M_\odot): [9, 10]$; binary mass ratio, $\log_{10}q: [-1, 0]$; GW frequency, $\log_{10}(f/\text{Hz}): [-9, -7.5]$; orbital inclination angle, $\cos i: [-1, 1]$; initial Earth-term phase, $\Phi_0: [0, 2\pi]$; and GW polarization angle, $\psi: [0, \pi]$. The simulated timing deviations include the pulsar terms with pulsar distances from Verbiest *et al.* [52] and allow for frequency evolution between the Earth and pulsar terms but not within the timing baseline of the data. We simulate 1500 binary signals and compute the signal-to-noise ratio (SNR) for each. We exclude realizations with $\text{SNR} < 5$ and $\text{SNR} > 15$, since our goal is to test our analysis approximation in moderate signal regimes where any biases would show, yet not so strong as to be unrealistic for PTAs. This leaves 342 injected-binary datasets remaining in the sample.

For each simulated dataset, we perform Bayesian analyses using the ENTERPRISE PTA software [44] and PTMCMCSampler [53] to sample the posterior distribution of the parameter space, employing uniform priors with ranges like above. We exclude high-frequency binaries from our simulations, because they are rare and unlikely to be detected due to limited sensitivity at higher frequencies [17–21]. Similarly, we inject only high-mass binaries, since PTAs are currently sensitive only to the most massive systems [31], to ensure high SNR, but our conclusions should also hold for lower-mass binaries. We perform two sets of analyses on each dataset: (i) The full signal model, which includes the pulsar terms (“PTerm” hereafter). This setup includes six binary parameters plus 90 pulsar parameters (pulsar distance, pulsar-term GW phase for each). To effectively sample the high-dimensional parameter space, we include dedicated Markov chain Monte Carlo (MCMC) proposal distributions designed for PTA SMBHB analyses [25]. (ii) A simplified model, which includes the Earth term but excludes all pulsar terms (“ETerm” hereafter). This setup needs only six parameters describing the circular binary waveform and does not use proposal distributions. Since we consider targeted GW searches (e.g., as in [37,39,40]), in both analyses, the sky position and distance of the source are fixed to the injected value. We also fix the per-pulsar red noise characteristics to injected values, as this will not alter the generality of our results.

Results.—In Fig. 1, we show an example of the marginalized posterior probability distributions for the total mass and GW frequency for a binary with $\text{SNR} \sim 9$. We see that both analyses successfully recover the injected values within 68% credibility and return similar constraints on these parameters. Next, we systematically examine how well the injected values X_{in} are recovered across all our simulated datasets, by calculating the percentage errors of

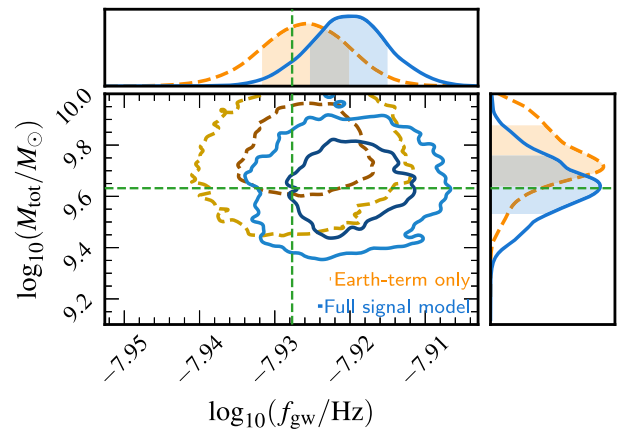


FIG. 1. Posterior distributions of the total mass and GW frequency. The ETerm and PTerm analyses are shown with orange dashed and blue solid lines, respectively, with green dashed lines showing the injected values. The shaded regions in the 1D posteriors show the 68% credible intervals.

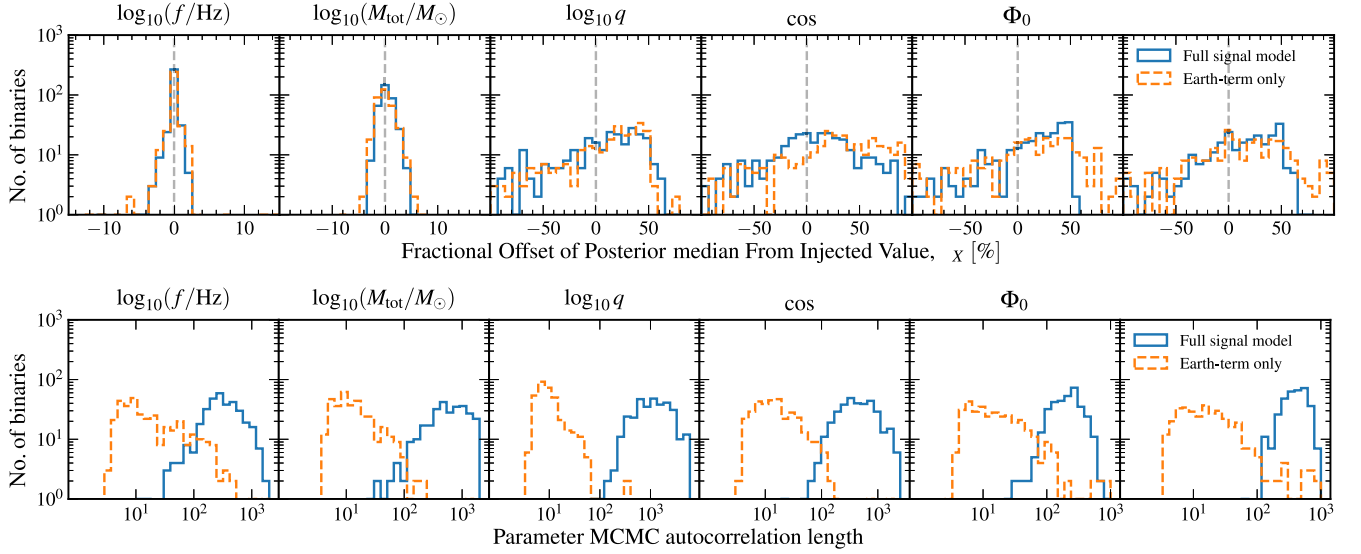


FIG. 2. Comparison of the ETerm (orange dashed lines) and PTerm (blue solid lines) analyses in terms of parameter estimation (top) and computational efficiency (bottom). Top: distribution of percent error δ_X (%) of the posterior median with respect to the injected value with vertical gray lines delineating 0%. Bottom: distribution of autocorrelation length L_x of the MCMC chains.

the posterior median $\delta_X = (X_{\text{in}} - X_{\text{post},50})/X_{\text{in}} \times 100\%$, where X is any of the six binary parameters. In the top panel of Fig. 2, we show the distribution of the percentage error for each binary parameter both with the ETerm (orange dashed lines) and PTerm (blue solid lines) analyses. In Table I, we show the 16th, 50th, and 84th percentiles of each error distribution. We also report the percentage of realizations, $P_{10\%}$, for which the posterior median is within 10% of the injected value, i.e., $|\delta_X| < 10\%$.

Both methods successfully recover the GW frequency and binary total mass, with narrow δ_X distributions peaked around 0% and high $P_{10\%}$ percentages. The PTerm analysis slightly outperforms the ETerm analysis in the case of the binary inclination, but even the PTerm analysis does not provide tight constraints, as evidenced by the wide distributions of δ_X and the relatively low $P_{10\%}$ percentages.

TABLE I. Percentiles (16th, 50th, and 84th) of the percent error distributions δ_X and fraction of realizations $P_{10\%}$, for which the median is within 10% of the injected value for each binary parameter and for each analysis.

Parameter	PTerm	ETerm	PTerm	ETerm
	δ_X (%)	δ_X (%)	$P_{10\%}$ (%)	$P_{10\%}$ (%)
$\log_{10} f$	0.0 ^{0.2} _{-0.2}	0.0 ^{0.4} _{-0.4}	99.7	97.4
$\log_{10} M_{\text{tot}}$	0.2 ^{1.6} _{-0.9}	-0.1 ^{1.5} _{-1.4}	100	100
$\log_{10} q$	-3.2 ^{37.0} _{-203.4}	1.5 ^{40.0} _{-188.5}	13.4	11.1
$\cos i$	5.3 ^{54.8} _{-59.2}	30.2 ^{83.2} _{-47.2}	17.5	7.3
Φ_0	2.9 ^{41.2} _{-245.2}	0.2 ^{46.6} _{-255.0}	11.7	12.3
ψ	-2.8 ^{41.9} _{-172.1}	-3.1 ^{46.1} _{-199.1}	15.2	15.2

Finally, the binary mass ratio, initial Earth-term phase, and GW polarization angle are poorly constrained in both analyses (see the Discussion section below). We note that, for multimessenger observations, the inclination and mass ratio may be independently constrained by the EM signal [34,36], and thus the simpler ETerm analysis may be sufficient even for these parameters [41].

The above metric for parameter-estimation fidelity relies on the posterior median, i.e., a point estimate, but the shape of the posterior distribution contains more information. We further compare the two analyses by calculating the Kullback-Leibler divergence D_{KL} , which measures the difference in information content between two distributions, a parameter's prior and posterior in our case (e.g., see Ref. [39] for a detailed description of this metric). A high value of D_{KL} shows more deviation of the posterior from the prior (and thus higher gain of information from the data), while a value of zero signifies identical distributions (i.e., the data did not update the prior information). In Table II, we report the median of the distribution of D_{KL} ratios between the two analyses, $R_{\text{KL}_x} = D_{\text{KL}_x}(\text{PTerm})/D_{\text{KL}_x}(\text{ETerm})$. Based on this ratio, we see that both analyses perform similarly for the GW frequency and binary total mass, with the PTerm returning on average 2% higher D_{KL} values for both parameters, consistent with our findings above. On the other hand, D_{KL} is ~ 25 times higher in the PTerm analysis for the mass ratio. This is driven by a large fraction of realizations ($\sim 65\%$) for which the posterior is almost identical to the prior (with $D_{\text{KL}} < 1$) in the ETerm analysis. For the remaining parameters, D_{KL} is on average higher for the ETerm analysis (again, see the Discussion section for more on this).

As a final test of the fidelity of the ETerm analysis for parameter estimation, we quantify potential biases using a

TABLE II. Median values for the distributions over simulations of the 68% credible interval ratio $R_{\Delta X}$, the KL Divergence ratio R_{KL} , and the autocorrelation length ratio R_L . The last two columns show the P_{68} and P_{95} values (ETerm|PTerm), i.e., the value for the ETerm analysis shown on the left and the respective value for the PTerm on the right.

Parameter	R_{KL}	R_L	P_{68}	P_{95}
$\log_{10} f$	1.02	24.7	67 71	88 94
$\log_{10} M_{\text{tot}}$	1.02	60.5	67 61	92 89
$\log_{10} q$	24.53	134.2	68 63	94 91
$\cos i$	0.92	30.7	68 76	89 97
Φ_0	0.28	16.2	65 68	85 95
ψ	0.39	27.2	65 70	82 95

p - p test. We assess the fraction of our simulated binary datasets for which the injected value falls within a given $p\%$ credible interval P_p , where unbiased coverage would return $P_p = p$. In Table II, we show the P_{68} and P_{95} values for both analyses. Both analyses perform similarly, providing unbiased parameter estimation, with P_{68} and P_{95} close to the expected values (within 3σ), with the exception of P_{95} for the initial phase and the GW polarization angle in the ETerm analysis. Since the searched signal in the ETerm analysis does not match the injected waveform, such deviations from the unbiased estimation are expected. Despite this, the bias is not significant, especially since some of these parameters may be independently constrained by the EM signal [34,36] and are not important for finding potential host galaxies.

Finally, we compare both methods in terms of computational efficiency. For this, we calculate the autocorrelation length L_X for each parameter X , which quantifies how often independent samples are drawn in the MCMC chains. In the bottom panel of Fig. 2, we show the distributions of L_X for the ETerm and PTerm analyses. Note that we thinned the chains by a factor of 10 and L_X is calculated in the final chains. In Table II, we report the median of the ratio of autocorrelation lengths between the two analyses $R_L = L_X(\text{PTerm})/L_X(\text{ETerm})$. We see that, depending on the parameter, the PTerm analysis requires between ~ 16 and 135 times more steps to draw independent samples. Finally, in order to ensure overall convergence in the analysis, every parameter needs to have enough independent samples, and thus the total length of the MCMC chain is determined by the chain with the longest L_X . In order to compare the efficiency of the two analyses, we calculate the maximum L_X among the six binary parameter chains L^{max} and then calculate the ratio of the maxima for the two analyses $R_{L^{\text{max}}} = L^{\text{max}}(\text{PTerm})/L^{\text{max}}(\text{ETerm})$. This provides an estimate of how much longer the PTerm analysis must be run in order to collect the same number of independent samples. The 16th, 50th, and 84th percentiles of the $R_{L^{\text{max}}}$ distribution are $68.6_{8.5}^{235.0}$. Therefore, we conclude that the ETerm analysis requires ~ 70 times fewer steps

and thus is ~ 70 times more efficient. We also compare the memory and CPU requirements of the above runs. On average, the PTerm analysis takes ~ 58 CPU hours to complete on an AMD Zen processor and requires ~ 1.8 GB of memory and ~ 0.5 GB of disk space to store the output chains. Compared to the ETerm, it is ~ 8 times more memory intensive, takes ~ 7 times longer to complete, and requires > 5 times more disk space. Beyond these quantitative comparisons, the ETerm is overall significantly simpler and easier to set up, e.g., it does not require highly tuned MCMC proposal distributions.

Discussion.—Searches for individually resolved supermassive black-hole binaries are among the most complicated and computationally expensive PTA analyses. So far, they have only been possible for a small number of targets [31,37,38]. The problem will be exacerbated in future PTA datasets, since the higher number of pulsars will inevitably increase the dimensionality of the parameter space and, in turn, the computational demands.

Currently, it is intractable to perform a systematic campaign of targeted searches for all SMBHB candidates identified in time-domain surveys (~ 250 systems) [36], and soon the vast photometric dataset of the Rubin Observatory will potentially uncover thousands of SMBHB candidates [46–48]. Similarly, the first PTA detection of an individually resolved binary—with its poor localization of potentially hundreds of square degrees—will allow for many potential host galaxies in its error volume [49]. Targeted multimessenger follow-ups of EM identified candidates or promising host galaxy candidates require efficient and reliable alternatives to the traditional pipeline. This led to the recent development of QuickCW [45], which delivers an accelerated Bayesian analysis by restructuring the exploration of the likelihood function.

Here we present a simpler possibility, which will enable systematic large-scale multimessenger studies of SMBHBs or rapid first assessments of candidates to determine their worthiness of a full pipeline follow-up. Our comprehensive comparison of targeted GW searches demonstrates that the simplified and significantly more efficient ETerm analysis can provide comparable constraints with the more complex and computationally demanding PTerm analysis. Both searches return similar constraints on the total mass and GW frequency of the binary, with the posterior median being within 10% of the injected value for the vast majority of realizations (over 97% for both analyses and both parameters). The remaining parameters are not particularly well constrained in either analysis, but the PTerm analysis performs slightly better for the orbital inclination. This is not a major limitation because the inclination and mass ratio may be independently constrained from the EM data for the case of EM candidates [36], while they are less important for host galaxy identification. Finally, neither analysis presents significant bias in the parameter recovery.

As mentioned, the initial Earth-term phase and GW polarization angle are not well constrained in either

analysis. These two parameters are degenerate, because signals with (Φ_0, ψ) and $(\Phi_0 + \pi, \psi + \pi/2)$ produce identical TOA deviations, which may result in bimodal 2D posterior distributions in these parameters. Such posteriors are observed in the PTerm analysis, but less often in the ETerm analysis. The tuned MCMC proposal distributions employed in the former likely force the sampler to more aggressively explore these parameters, whereas in the minimally tuned ETerm analysis, the sampler may get stuck in one of the modes. The bimodality of posteriors in the PTerm analysis can explain the lower D_{KL} values; the ETerm posteriors are more peaked and thus deviate more from the uniform prior distributions. Similarly, the inability to capture the bimodality of the posteriors can explain the slight deviations in the p - p test for these parameters in the ETerm analysis.

Finally, we note that, while we performed realistic simulations of near-future PTA sensitivity based on the NANOGrav 12.5-yr dataset, we only injected GW signals from single resolvable binaries. Such binaries will be detected after the GW background [17–21], evidence for which is already present in current datasets [7–10]. In future simulations, we will also explore the modifications needed (if any) for the implementation of our technique in the presence of a stochastic GW background and in the presence of signals from other resolvable binaries.

Summary.—With realistic simulations that emulate near-future PTA sensitivity, we compared the performance of targeted GW searches using a full signal analysis, PTerm, and a simpler and faster ETerm approximation, which neglects the pulsar terms. This collapses the parameter space that must be searched over by twice the number of pulsars, which for modern PTAs is $\gtrsim 50$. We found that the ETerm analysis provides similar constraints on the binary total mass and GW frequency—the most important properties for multimessenger assessment—and is ~ 70 times more efficient as a result of the collapsed search-space dimensionality. This analysis acceleration empowers the rigorous targeted examination of large samples of candidate SMBHB systems, many of which have already been found and many more of which are promised by the advent of new time-domain surveys like LSST. This method can also be applied to selected promising host galaxies in the large error volume of the first individually resolved binary detected by PTAs.

The output of our simulations can be found in [54].

We thank Nihan Pol, Polina Petrov, William Lamb, and our colleagues in NANOGrav and the International Pulsar Timing Array for fruitful discussions and feedback during the development of this technique. M. C., S. R. T., and J. R. acknowledge support from NSF AST-2007993. S. R. T. also acknowledges support from the NANOGrav NSF Physics Frontier Center No. 2020265 and an NSF

CAREER No. 2146016. C. A. W. acknowledges support from CIERA, the Adler Planetarium, and the Brinson Foundation through a CIERA-Adler postdoctoral fellowship. This work was conducted in part using the resources of the Advanced Computing Center for Research and Education (ACCRE) at Vanderbilt University, Nashville, TN. This work was performed in part at Aspen Center for Physics, which is supported by National Science Foundation Grant No. PHY-2210452.

*maria.charisi@nanograv.org

- [1] M. A. McLaughlin, The North American nanohertz observatory for gravitational waves, *Classical Quantum Gravity* **30**, 224008 (2013).
- [2] S. Ransom, A. Brazier, S. Chatterjee, T. Cohen, J. M. Cordes, M. E. DeCesar, P. B. Demorest, J. S. Hazboun, M. T. Lam, R. S. Lynch, M. A. McLaughlin, S. M. Ransom, X. Siemens, S. R. Taylor, and S. J. Vigeland, The NANOGrav program for gravitational waves and fundamental physics, *Bull. Am. Assoc. Am. Assoc.* **51**, 195 (2019), <https://baas.aas.org/pub/2020n7i195/release/1>.
- [3] M. Kramer and D. J. Champion, The European pulsar timing array and the large European array for pulsars, *Classical Quantum Gravity* **30**, 224009 (2013).
- [4] R. N. Manchester, The Parkes pulsar timing array project, in *40 Years of Pulsars: Millisecond Pulsars, Magnetars and More*, American Institute of Physics Conference Series Vol. 983, edited by C. Bassa, Z. Wang, A. Cumming, and V. M. Kaspi (2008), pp. 584–592, <https://ui.adsabs.harvard.edu/abs/2008AIPC..983..584M/abstract>.
- [5] G. Hobbs, The Parkes pulsar timing array, *Classical Quantum Gravity* **30**, 224007 (2013).
- [6] K. J. Lee, Prospects of gravitational wave detection using pulsar timing array for Chinese future telescopes, in *Frontiers in Radio Astronomy and FAST Early Sciences Symposium 2015*, Astronomical Society of the Pacific Conference Series Vol. 502, edited by L. Qain and D. Li (2016), p. 19, <https://ui.adsabs.harvard.edu/abs/2016ASPC..502...19L/abstract>.
- [7] G. Agazie *et al.* (Nanograv Collaboration), The NANOGrav 15 yr data set: Evidence for a gravitational-wave background, *Astrophys. J. Lett.* **951**, L8 (2023).
- [8] J. Antoniadis *et al.*, The second data release from the European pulsar timing array III. Search for gravitational wave signals, *Astron. Astrophys.* **678**, A50 (2023).
- [9] D. J. Reardon *et al.*, Search for an isotropic gravitational-wave background with the Parkes pulsar timing array, *Astrophys. J. Lett.* **951**, L6 (2023).
- [10] H. Xu *et al.*, Searching for the nano-hertz stochastic gravitational wave background with the Chinese pulsar timing array data release I, *Res. Astron. Astrophys.* **23**, 075024 (2023).
- [11] R. W. Hellings and G. S. Downs, Upper limits on the isotropic gravitational radiation background from pulsar timing analysis, *Astrophys. J. Lett.* **265**, L39 (1983).
- [12] G. Agazie *et al.* (Nanograv Collaboration), The NANOGrav 15 yr data set: Constraints on supermassive black hole

- binaries from the gravitational-wave background, *Astrophys. J. Lett.* **952**, L37 (2023).
- [13] J. Antoniadis *et al.*, The second data release from the European pulsar timing array: V. Implications for massive black holes, dark matter and the early Universe, [arXiv:2306.16227](https://arxiv.org/abs/2306.16227).
- [14] A. De Rosa *et al.*, The quest for dual and binary supermassive black holes: A multi-messenger view, *New Astron. Rev.* **86**, 101525 (2019).
- [15] S. Burke-Spolaor, S. R. Taylor, M. Charisi, T. Dolch, J. S. Hazboun, A. M. Holgado, L. Z. Kelley, T. J. W. Lazio, D. R. Madison, N. Mc Mann, C. M. F. Mingarelli, A. Rasskazov, X. Siemens, J. J. Simon, and T. L. Smith, The astrophysics of nanohertz gravitational waves, *Astron. Astrophys. Rev.* **27**, 5 (2019).
- [16] S. R. Taylor, The nanohertz gravitational wave astronomer, [arXiv:2105.13270](https://arxiv.org/abs/2105.13270).
- [17] P. A. Rosado, A. Sesana, and J. Gair, Expected properties of the first gravitational wave signal detected with pulsar timing arrays, *Mon. Not. R. Astron. Soc.* **451**, 2417 (2015).
- [18] C. M. F. Mingarelli, T. J. W. Lazio, A. Sesana, J. E. Greene, J. A. Ellis, C.-P. Ma, S. Croft, S. Burke-Spolaor, and S. R. Taylor, The local nanohertz gravitational-wave landscape from supermassive black hole binaries, *Nat. Astron.* **1**, 886 (2017).
- [19] L. Z. Kelley, L. Blecha, L. Hernquist, A. Sesana, and S. R. Taylor, Single sources in the low-frequency gravitational wave sky: Properties and time to detection by pulsar timing arrays, *Mon. Not. R. Astron. Soc.* **477**, 964 (2018).
- [20] S. R. Taylor, R. van Haasteren, and A. Sesana, From bright binaries to bumpy backgrounds: Mapping realistic gravitational wave skies with pulsar-timing arrays, *Phys. Rev. D* **102**, 084039 (2020).
- [21] B. Bécsy, N. J. Cornish, and L. Z. Kelley, Exploring realistic nanohertz gravitational-wave backgrounds, *Astrophys. J.* **941**, 119 (2022).
- [22] Z. Arzoumanian *et al.* (NANOGrav Collaboration), Gravitational waves from individual supermassive black hole binaries in circular orbits: Limits from the North American nanohertz observatory for gravitational waves, *Astrophys. J.* **794**, 141 (2014).
- [23] X.-J. Zhu, G. Hobbs, L. Wen, W. A. Coles, J.-B. Wang, R. M. Shannon, R. N. Manchester, M. Bailes, N. D. R. Bhat, S. Burke-Spolaor, S. Dai, M. J. Keith, M. Kerr, Y. Levin, D. R. Madison, S. Osłowski, V. Ravi, L. Toomey, and W. van Straten, An all-sky search for continuous gravitational waves in the Parkes pulsar timing array data set, *Mon. Not. R. Astron. Soc.* **444**, 3709 (2014).
- [24] S. Babak *et al.*, European pulsar timing array limits on continuous gravitational waves from individual supermassive black hole binaries, *Mon. Not. R. Astron. Soc.* **455**, 1665 (2016).
- [25] K. Aggarwal *et al.* (The NANOGrav Collaboration), The NANOGrav 11 yr data set: Limits on gravitational waves from individual supermassive black hole binaries, *Astrophys. J.* **880**, 116 (2019).
- [26] M. Falxa *et al.* (IPTA Collaboration), Searching for continuous gravitational waves in the second data release of the international pulsar timing array, *Mon. Not. R. Astron. Soc.* **521**, 5077 (2023).
- [27] G. Agazie *et al.* (Nanograv Collaboration), The NANOGrav 15 yr data set: Bayesian limits on gravitational waves from individual supermassive black hole binaries, *Astrophys. J. Lett.* **951**, L50 (2023).
- [28] Z. Arzoumanian *et al.* (Nanograv Collaboration), The NANOGrav 12.5 yr data set: Bayesian limits on gravitational waves from individual supermassive black hole binaries, *Astrophys. J. Lett.* **951**, L28 (2023).
- [29] J. Antoniadis *et al.*, The second data release from the European pulsar timing array IV. Search for continuous gravitational wave signals, [arXiv:2306.16226](https://arxiv.org/abs/2306.16226).
- [30] K. Schutz and C.-P. Ma, Constraints on individual supermassive black hole binaries from pulsar timing array limits on continuous gravitational waves, *Mon. Not. R. Astron. Soc.* **459**, 1737 (2016).
- [31] Z. Arzoumanian *et al.* (Nanograv Collaboration), The NANOGrav 11 yr data set: Limits on supermassive black hole binaries in galaxies within 500 Mpc, *Astrophys. J.* **914**, 121 (2021).
- [32] V. Springel, T. Di Matteo, and L. Hernquist, Black holes in galaxy mergers: The formation of red elliptical galaxies, *Astrophys. J. Lett.* **620**, L79 (2005).
- [33] T. Bogdanović, M. C. Miller, and L. Blecha, Electromagnetic counterparts to massive black-hole mergers, *Living Rev. Relativity* **25**, 3 (2022).
- [34] D. J. D’Orazio and M. Charisi, Observational signatures of supermassive black hole binaries, [arXiv:2310.16896](https://arxiv.org/abs/2310.16896).
- [35] L. Kelley *et al.* (Nanograv Collaboration), Multi-messenger astrophysics with pulsar timing arrays, *Bull. Am. Astron. Soc.* **51**, 490 (2019), <https://baas.aas.org/pub/2020n3i490/release/1>.
- [36] M. Charisi, S. R. Taylor, J. Runnoe, T. Bogdanovic, and J. R. Trump, Multimessenger time-domain signatures of supermassive black hole binaries, *Mon. Not. R. Astron. Soc.* **510**, 5929 (2022).
- [37] Z. Arzoumanian *et al.* (NANOGrav Collaboration), Multi-messenger gravitational-wave searches with pulsar timing arrays: Application to 3C 66B using the NANOGrav 11-year data set, *Astrophys. J.* **900**, 102 (2020).
- [38] G. Agazie *et al.*, The NANOGrav 12.5-year data set: Multi-messenger targeted search for gravitational waves from an eccentric supermassive binary in 3C 66B, [arXiv:2309.17438](https://arxiv.org/abs/2309.17438).
- [39] T. Liu and S. J. Vigeland, Multi-messenger approaches to supermassive black hole binary detection and parameter estimation: Implications for nanohertz gravitational wave searches with pulsar timing arrays, *Astrophys. J.* **921**, 178 (2021).
- [40] T. Liu, T. Cohen, C. McGrath, P. B. Demorest, and S. J. Vigeland, Multi-messenger approaches to supermassive black hole binary detection and parameter estimation. II. Optimal strategies for a pulsar timing array, *Astrophys. J.* **945**, 78 (2023).
- [41] M. Charisi *et al.*, Improved parameter estimation of supermassive black hole binaries through combined time-domain and pulsar timing array observations (to be published).
- [42] V. Corbin and N. J. Cornish, Pulsar timing array observations of massive black hole binaries, [arXiv:1008.1782](https://arxiv.org/abs/1008.1782).

- [43] K. J. Lee, N. Wex, M. Kramer, B. W. Stappers, C. G. Bassa, G. H. Janssen, R. Karuppusamy, and R. Smits, Gravitational wave astronomy of single sources with a pulsar timing array, *Mon. Not. R. Astron. Soc.* **414**, 3251 (2011).
- [44] J. A. Ellis, M. Vallisneri, S. R. Taylor, and P. T. Baker, ENTERPRISE: Enhanced numerical toolbox enabling a robust pulsar inference suite (2019), ascl:1912.015, <https://ui.adsabs.harvard.edu/abs/2019ascl.soft12015E/abstract>.
- [45] B. Bécsy, N. J. Cornish, and M. C. Digman, Fast Bayesian analysis of individual binaries in pulsar timing array data, *Phys. Rev. D* **105**, 122003 (2022).
- [46] C. Xin and Z. Haiman, Ultra-short-period massive black hole binary candidates in LSST as LISA “verification binaries”, *Mon. Not. R. Astron. Soc.* **506**, 2408 (2021).
- [47] L. Z. Kelley, D. J. D’Orazio, and R. Di Stefano, Gravitational self-lensing in populations of massive black hole binaries, *Mon. Not. R. Astron. Soc.* **508**, 2524 (2021).
- [48] C. A. Witt, M. Charisi, S. R. Taylor, and S. Burke-Spolaor, Quasars with periodic variability: capabilities and limitations of Bayesian searches for supermassive black hole binaries in time-domain surveys, *Astrophys. J.* **936**, 89 (2022).
- [49] J. M. Goldstein, A. Sesana, A. M. Holgado, and J. Veitch, Associating host galaxy candidates to massive black hole binaries resolved by pulsar timing arrays, *Mon. Not. R. Astron. Soc.* **485**, 248 (2019).
- [50] N. S. Pol *et al.* (Nanograv Collaboration), Astrophysics milestones for pulsar timing array gravitational-wave detection, *Astrophys. J. Lett.* **911**, L34 (2021).
- [51] M. F. Alam *et al.* (Nanograv Collaboration), The NANOGrav 12.5 yr data set: Observations and narrowband timing of 47 millisecond pulsars, *Astrophys. J. Suppl. Ser.* **252**, 4 (2021).
- [52] J. P. W. Verbiest, J. M. Weisberg, A. A. Chael, K. J. Lee, and D. R. Lorimer, On pulsar distance measurements and their uncertainties, *Astrophys. J.* **755**, 39 (2012).
- [53] J. Ellis and R. van Haasteren, PTMCMCSampler: Parallel tempering MCMC sampler package written in Python (2017), <https://ui.adsabs.harvard.edu/abs/2019ascl.soft12017E/abstract>.
- [54] <https://github.com/mariacharisi/Earth-Term-MMA.git>.